

Superconductivity enhancement in the S-doped Weyl semimetal candidate MoTe₂

F. C. Chen^{1,2}, X. Luo^{1*}, R. C. Xiao^{1,2}, W.J. Lu¹, B. Zhang⁵, H.X. Yang⁵, J. Q. Li^{5,6},
Q. L. Pei¹, D. F. Shao¹, R. R. Zhang³, L. S. Ling³, C. Y. Xi³, W. H. Song¹ and Y. P. Sun^{3,1,4*}

¹ Key Laboratory of Materials Physics, Institute of Solid State Physics, Chinese Academy of Sciences, Hefei, 230031, China

² University of Science and Technology of China, Hefei, 230026, China

³ High Magnetic Field Laboratory, Chinese Academy of Sciences, Hefei, 230031, China

⁴ Collaborative Innovation Center of Advanced Microstructures, Nanjing University, Nanjing, 210093, China

⁵ Beijing National Laboratory for Condensed Matter Physics, Institute of Physics, Chinese Academy of Sciences, Beijing, 100190, China

⁶ Collaborative Innovation Center of Quantum Matter, Beijing, 100190, China

Abstract

Two-dimensional (2D) transition-metal dichalcogenide (TMDs) MoTe₂ has attracted much attention due to its predicted Weyl semimetal (WSM) state and a quantum spin Hall insulator in bulk and monolayer form, respectively. We find that the superconductivity in MoTe₂ single crystal can be much enhanced by the partial substitution of the Te ions by the S ones. The maximum of the superconducting temperature T_C of MoTe_{1.8}S_{0.2} single crystal is about 1.3 K. Compared with the parent MoTe₂ single crystal ($T_C=0.1$ K), nearly 13-fold in T_C is improved in MoTe_{1.8}S_{0.2} one. The superconductivity has been investigated by the resistivity and magnetization measurements. MoTe_{2-x}S_x single crystals belong to weak coupling superconductors and the improvement of the superconductivity may be related to the enhanced electron-phonon coupling induced by the S-ion substitution. A dome-shape superconducting phase diagram is obtained in the S-doped MoTe₂ single crystals. MoTe_{2-x}S_x materials may provide a new platform for our understanding of superconductivity phenomena and topological physics in TMDs.

* Corresponding author: xluo@issp.ac.cn and ypsun@issp.ac.cn

I Introduction

Layered transition-metal dichalcogenides (TMDs) materials, named as MX_2 , where M is a transition metal (Ta, Mo and W) and X is a chalcogen (S, Se and Te), have attracted renewed interest owing to their rich physical properties and promising potential applications.[1-10] For example, artificial van der Waals heterostructures with high on/off current ratio in TMDs are promising as an active channel for next-generation devices.[2] Topological field-effect transitions based on quantum spin Hall (QSH) insulators are novel type of device.[9] At the same time, charge-density waves and superconductivity have also been observed in TMDs.[10] Particularly, a dome-shaped superconducting phase diagram is observed in a gate-tuned MoS_2 device and the WTe_2 bulk crystal driven by the pressure.[4-6]

Recently, MoTe_2 has been attracted much attention because it was predicted a new type-II Weyl semimetal (WSM) candidate.[11] MoTe_2 crystalizes into three different phases: 2H, 1T' and T_d ones. The 2H phase shows a semiconducting behavior. On the other hand, the 1T' and T_d phases present semi-metallic and exhibit pseudo-hexagonal layers with zig-zag metal chains. The T_d compound can be obtained by cooling the 1T' phase down to 245 K.[8, 12] The T_d phase of MoTe_2 , which is isostructural to WTe_2 , is predicted to be a candidate WSM.[13] Very recently, the T_d - MoTe_2 is reported to be a superconductivity with $T_C=0.1$ K, the small applied pressure can dramatically enhance the T_C and a dome-shaped superconducting phase diagram under the applied pressure is observed.[8] The MoTe_2 opens a door to study the interaction of topological physics and superconductivity in the bulk materials. Provoked by above reported work, since the superconductivity can be much enhanced by the applied pressure in MoTe_2 bulk crystal, which implies that the T_d - MoTe_2 may be also sensitive to the chemical pressure induced by the ion substitution. In this work, we did the partial substitution of Te ions by S ones in MoTe_2 single crystal. The enhanced superconducting temperature T_C is observed and the maximum of the T_C in $\text{MoTe}_{1.8}\text{S}_{0.2}$ single crystals about 1.3 K. A dome-shape superconducting phase diagram is obtained in $\text{MoTe}_{2-x}\text{S}_x$ single crystals and the possible reasons of the enhanced superconductivity have been discussed. The $\text{MoTe}_{2-x}\text{S}_x$ materials may provide a new platform to understand the superconductivity phenomena and topological physics in TMDs.

II Experimental details

MoTe₂ and MoTe_{2-x}S_x (0 ≤ x ≤ 1) single crystals were grown by the chemical vapor transport method using polycrystalline MoTe₂ and MoTe_{2-x}S_x as raw materials and I₂ as a transport agent. Firstly, we made the polycrystalline MoTe₂ and MoTe_{2-x}S_x (0 ≤ x ≤ 1). Mo (Alfa Aesar, 99.9 %) and Te or S (Alfa Aesar, 99.9 %) powders with a stoichiometric ratio were ground, pressed into pellets, and put in an evacuated quartz tube. All were done in an Ar-filled glove box. The sealed quartz tube was heated to 800 °C for 20 hours and kept for 7 days, then quenched to ice water. The polycrystalline MoTe₂ or MoTe_{2-x}S_x and the agent I₂ were mixed and sealed into another evacuated quartz tubes. The sealed quartz tubes were put in a two-zone tube furnace. The crystal growth recipe is followed the reported paper.[12] The hot side is about 1000 °C and the cold side is 900 °C, and dwelled for 7 days. In order to improve the quality of single crystals, we quenched the quartz tubes into ice-water as soon as possible before the growth sequence ending. Plate-like shape single crystals with shining surfaces were obtained. The size of the crystal was about 4*4*0.5 mm³. The single crystals were air-stable and can be easily exfoliated. Powder X-ray diffraction (XRD) patterns were taken with Cu K_{α1} radiation (λ=0.15406 nm) using a PANalytical X'pert diffractometer at room temperature. The element analysis of the single crystals was performed using a commercial energy dispersive spectroscopy (EDS) microprobe. The element compositions of the single crystals used in the text are the ones obtained from EDS measurements. The magnetic properties were carried out by the magnetic property measurement system with a ³He cryostat (MPMS-XL7). The electrical transport measurements were performed in a ⁴He cryostat from 300 K to 2 K, and in a ³He cryostat down to 0.35 K by a four-probe method to eliminate the contact resistance. The measurement of specific heat was carried out by a heat-pulse relaxation method on Physical Properties Measurement System (PPMS-9T). Raman spectra were measured on Horiba T64000, with excitation wavelength 647.4 nm and the power density was kept below 20 mW cm⁻² in order to minimize the heating effects. The density functional theory (DFT) calculations were carried out using QUANTUM ESPRESSO package [14] with ultrasoft pseudopotentials. The exchange-correlation interaction was treated with the generalized gradient approximation (GGA) with Perdew-Burke-Ernzerh (PBE) of parametrization.[15] The energy cutoff for the plane-wave basis set was 65 Ry. The Vanderbilt-Marzari Fermi smearing method with a smearing parameter of σ = 0.02 Ry was used for the calculations of the total energy and electron charge density. The van der Waals interactions were treated by a semiempirical dispersion

correction scheme (DFT-D).[16, 17] The crystal structures were optimized with respect to lattice parameters and atomic positions. Brillouin zone sampling is performed on the Monkhorst-Pack (MP) meshes [18] of $6 \times 12 \times 4$ for structure relaxation and $12 \times 24 \times 8$ for density of states (DOS) calculation. Electron diffraction and scanning transmission electron microscopy (STEM) experiments were performed in the JEOL ARM200F equipped with double aberration correctors and cold field emission gun operated at 200kV.

III Results and Discussion

MoTe₂ crystallizes into three different phases, as shown in Fig. 1 (a)-(c). In 2H phase, the Mo atom has trigonal prismatic coordination with the Te atoms. The 1T' phase (space group $P2_1/m$), which is also called β -phase, is a monoclinic lattice and is stable at room temperature. The T_d phase (space group $Pmn2_1$) is an orthorhombic lattice and the 1T' one is slight sliding of layer-stacking of the T_d phase. We selected MoTe_{1.8}S_{0.2} single crystal as a typical sample to do the detailed experiments. Figure 1 (d) shows the X-ray patterns of MoTe_{1.8}S_{0.2} single crystals along [001] direction. We did the powder X-ray of crushed MoTe_{1.8}S_{0.2} single crystals. However, we found that the X-ray data can be well fitted based on the orthorhombic or monoclinic symmetry, as shown in Fig. S1. It is difficult for us to distinguish the structure of MoTe_{1.8}S_{0.2} single crystal at the room temperature. We also carried out TEM characterization of the MoTe_{1.8}S_{0.2} single crystal. As shown in Fig. 1 (e), the diffraction spots on the [001] selected area electron diffraction (SAED) pattern can be well indexed by the orthorhombic or monoclinic symmetry. However, the SAED pattern (Fig. 1(f)) and annular bright field (ABF) STEM image (Fig. 1(g)) taken along the [010] zone axis direction demonstrate evident structure difference comparing with the previous reported orthorhombic or monoclinic structure, it is recognizable that the MoTe(S)X₆ octahedral are much less distorted.

In order to compare the lattice parameters of MoTe₂ and MoTe_{1.8}S_{0.2} single crystals, we also did the XRD experiment of the crushed MoTe₂ single crystals. Figure S2 shows the experimental and calculated XRD patterns. The calculated lattice parameters of crushed MoTe₂ and MoTe_{1.8}S_{0.2} single crystals and the reported MoTe₂ one are summarized in Table I of the supporting materials. In addition, in order to get more some structural information on the MoTe_{2-x}S_x single crystal, we also did the Raman experiments. As shown in Fig. S3, except for MoTeS single crystal (changing

into 2H phase), all another crystals show similar Raman signals at room temperature. The temperature dependence of Raman spectra of the MoTe₂ single crystal is shown in Fig. S4, it seems that it is even difficult to tell the phase transition from present Raman experiments. That means we still can't tell the structure of S-doped MoTe₂ crystals. Thus, more detailed experiments are really needed to perform in the future.

Figure 2 shows the evolution of the resistance as a function of temperature $\rho(T)$ in a MoTe_{1.8}S_{0.2} single crystal down to 0.35 K. For the MoTe₂ single crystal, we did the measurement down to 2 K under the cooling and warming modes. As shown in Fig. 2, an anomaly with a hysteresis in the $\rho(T)$ of MoTe₂ single crystals observed, which is associated with the first-order structural phase transition from 1T' phase to T_d phase around 240 K and consistent with the reported results.[8,12] We applied the Fermi-liquid model $\rho(T)=\rho_0+A*T^2$, which ρ_0 and A are the residual resistivity and a constant, respectively, to the curve below 50 K as shown in the left inset of Fig. 2. The model analysis yielded the residual resistivity ρ_0 of $1.36*10^{-4}$ Ω cm and the coefficient A of 0.00238 $\mu\Omega$ cm, indicating Fermi-liquid-like behavior for MoTe₂ single crystal. For MoTe_{1.8}S_{0.2} single crystal, as shown in the right inset of Fig. 2, a clear zero-resistivity behavior is observed around 1.3 K. We measured the $\rho(T)$ under applied magnetic field H=0.5 T, the zero-resistivity temperature moves to 0.7 K, which indicates the superconductivity may occurs in MoTe_{1.8}S_{0.2} single crystal. On the other hand, we also find that there exists the minimum of the resistivity around $T_{min}=8$ K before the superconducting transition in MoTe_{1.8}S_{0.2} single crystal, which is similar to the transport properties of the WTe₂ single crystal under the applied high pressure.[5] The presence of the minimum of resistivity may be related to the structural abnormalities induced by the substitution of Te ions by S ones in MoTe_{1.8}S_{0.2} single crystal.

To test the superconductivity of MoTe_{1.8}S_{0.2} single crystal further, we did the magnetic measurements. Figure 3 presents the temperature dependence of magnetization $M(T)$ with the zero-field and field cooling (ZFC and FC) modes under an applied magnetic field of 10 Oe. The diamagnetic signal, in other words, the superconducting transition, can be obviously seen at $T_C=1.3$ K in the left inset of Fig. 3, which is in good agreement with the resistance measurements. The calculated shielding superconducting volume fraction at 0.5 K is about 60 %, which means the bulk superconducting behavior of the MoTe_{1.8}S_{0.2} single crystal. The magnetization as a function of magnetic fields at 0.5 K is shown in the right inset of Fig. 3. The clear hysteresis is

observed, which indicates a typical type-II superconducting behavior of MoTe_{1.8}S_{0.2} single crystals. Compared with the parent MoTe₂ ($T_C=0.1$ K), nearly 13-fold of the superconducting temperature is observed in S doped MoTe_{1.8}S_{0.2} single crystal.

The temperature dependence of specific heat C_P also provides more information about the normal state properties. Figure 4 shows the temperature dependence of the heat capacity C_P of MoTe₂ and MoTe_{1.8}S_{0.2} single crystals at $H=0$ above T_C . C_P/T varies almost linearly with T^2 . The Sommerfeld constant γ_N is obtained from the fit $C_P/T = \gamma_N + \beta T^2$ (γ_N and β are T -independent coefficients), where γ_N is the normal-state electronic contribution and β is the lattice contribution to the specific heat. The fitting results yield $\gamma_N = 3.06\text{mJ mol}^{-1} \text{K}^{-2}$ and $\beta = 0.758\text{mJ mol}^{-1} \text{K}^{-4}$ for MoTe₂ single crystal and $\gamma_N = 2.07\text{mJ mol}^{-1} \text{K}^{-2}$ and $\beta = 0.635\text{mJ mol}^{-1} \text{K}^{-4}$ for MoTe_{1.8}S_{0.2} one, respectively. The resulted DOS at Fermi surface $N(E_F)$ are 1.33 states/e V and 0.88 states/eV for MoTe₂ and MoTe_{1.8}S_{0.2} single crystals, respectively. The Debye temperature Θ_D can be determined from the coefficient of the T^2 term $\beta = N(12/5)\pi^4 R \Theta_D^{-3}$, where $R = 8.314 \text{ J mol}^{-1} \text{K}^{-1}$ and $N = 3$ for the MoTe₂ and MoTe_{1.8}S_{0.2} single crystals. The Debye temperatures Θ_D are 135 K and 143 K for MoTe₂ and MoTe_{1.8}S_{0.2} single crystals, respectively. All the fitting results are summarized in **Table I**. An estimation of the strength of the electron-phonon coupling (EPC) can be derived from the McMillan formula: [19, 20]

$$\lambda_{ep} = \frac{\mu^* \ln\left(\frac{1.45T_C}{\Theta_D}\right) - 1.04}{1.04 + \ln\left(\frac{1.45T_C}{\Theta_D}\right)(1 - 0.62\mu^*)} \quad . \quad (1)$$

By assuming the Coulomb pseudopotential $\mu^* = 0.1$, the EPC constant λ_{ep} is estimated to be 0.32 and 0.49 for MoTe₂ and MoTe_{1.8}S_{0.2} single crystals, respectively. The calculated EPC show that both of MoTe₂ and MoTe_{1.8}S_{0.2} single crystals are weak coupling superconductors.[19] Because the $N(E_F)$ of MoTe₂ single crystal is larger than that of MoTe_{1.8}S_{0.2} one, the improvement of the superconductivity in MoTe_{1.8}S_{0.2} single crystal can't be explained according to the variation of DOS of Fermi surface $N(E_F)$ and it may be related to the enhancement of the EPC by the S-ion substitution.

In order to study the superconducting evolution with S-doping level, we also grew and studied the electrical transport properties of the MoTe_{2-x}S_x ($0 \leq x \leq 1$) single crystals. All the zero-resistivity temperature T_C , the minimum temperature of the resistivity T_{min} and the structural phase transition temperature T_S vs. the doped S contents x are summarized in the T - x phase

diagram shown in Fig. 5. The structural phase transition temperature T_S is defined from the $\rho(T)$ data and similar to that of MoTe₂ single crystal,[12] as shown in the inset of Fig. S5 (a). Note that the T_S anomaly slowly increases with the little S-doped content x , then decreases rapidly with the increasing x . Further, the T_S disappears at $x=0.18$. For the superconducting temperature T_C , it increases is nearly linearly up to a maximum $T_C=1.3$ at $x=0.2$, as shown in Fig. S6. From this maximum, the T_C begins to decrease with increasing x , with the transition eventually disappearing at $x=0.37$. Thus, a dome-shaped superconducting phase diagram is obtained for MoTe_{2-x}S_x single crystal. For the S doped MoTe_{2-x}S_x crystals, the lower S-doping at Te sites can sharply increase in T_C , which is concomitant with enhancement of structural transition. Then, the T_C increases still slowly, however, the T_S is suppressed and disappearing with the increasing x , which are similar to with the results from the applied pressure in MoTe₂ single crystal.[8] On the other hand, when the content x is larger than 0.18, which is in accord with the content where the structural phase disappears, the minimum of resistivity T_{min} presents and increases slowly with the x , then tends to a constant value when the x is larger or equal to 0.37. For x is equal to 1, the crystal presents 2H phase and shows a semiconducting behavior, as shown in Fig. S3 and S5. However, we did not get the single crystals when x is larger than 1, which means the solution limit of S ions may be $x=1$ in MoTe_{2-x}S_x single crystals.

To understand the enhanced superconductivity in MoTe_{2-x}S_x single crystals, we did the first principle calculations. In order to simulate the S-doping effect, we substitute one Te atom in MoTe₂ unit cell by one S atom, i.e., the doped MoTe_{7/4}S_{1/4} was theoretically considered. The results show that the GGA slightly overestimates the lattice parameters of MoTe₂ with 1T' and T_d structures compared with those obtained from experiments (see **Table I** in the supporting materials, the difference is less than 2%). For the MoTe_{7/4}S_{1/4} sample, we test the cases that S atom locates at four inequivalent Te-sites in the unit cell respectively. By comparing the total energies, we found both in 1T' and T_d structure, S atom tends to replace the Te atom for forming the shortest Mo-Te bond. As expected, the S substitution makes the structures shrinking. Figure S7 shows the calculated DOS for MoTe₂ and MoTe_{7/4}S_{1/4} with 1T' and T_d structures. For the MoTe₂, our calculation is well consistent with previous calculations.[21] One can note that in both structures S doping rarely changes the overall structure of DOS. S doping slightly increases the band widths, which should be due to the enhanced p - d hybridization in the shrunked structures. In both structures

the DOS at E_F ($N(E_F)$) decreases upon S doping, as shown in Fig. S5 (c), which is good agreement with the results from the C_P measurements. That is, the value of Sommerfeld constant γ_N of $\text{MoTe}_{1.8}\text{S}_{0.2}$ crystal is lower than that of MoTe_2 one. Therefore, the decreased $N(E_F)$ does not support the S-doping induced superconductivity enhancement in 1T' and T_d structures and consistent with the results from the experimental results. The real structure of our experimentally prepared $\text{MoTe}_{2-x}\text{S}_x$ crystals might be different from 1T' and T_d , which needs to be further investigated both in experiment and theory.

Now, we pay attention to the EPC strength λ_{ep} . As we known, the EPC strength λ_{ep} for a material can be qualitatively expressed as:

$$\lambda_{ep} = \sum_{\alpha} \frac{\langle I_{\alpha}^2 \rangle N_{\alpha}(E_F)}{M_{\alpha} \langle \omega_{\alpha}^2 \rangle}, \quad (2)$$

where the $\langle I_{\alpha}^2 \rangle$, M_{α} , and $\langle \omega_{\alpha}^2 \rangle$ are the mean square EPC matrix element averaged over Fermi surface, atomic mass, and averaged squared phonon frequency of the α th atom in the unit cell, respectively.[22-24] We can simply compare the variations of $\langle I_{\alpha}^2 \rangle$, M_{α} , $\langle \omega_{\alpha}^2 \rangle$ and $N(E_F)$ of MoTe_2 and $\text{MoTe}_{1.8}\text{S}_{0.2}$ crystals. As we know, the S ions are lighter than Te one, so the M_{α} of $\text{MoTe}_{1.8}\text{S}_{0.2}$ single crystal (332.03 g/mol) is smaller than that of MoTe_2 one (351.14 g/mol). Meanwhile, the Debye temperature Θ_D is in proportion to the phonon frequency $\langle \omega_{\alpha}^2 \rangle$ and that of $\text{MoTe}_{1.8}\text{S}_{0.2}$ crystal ($\Theta_D=143$ K) is little larger than that of MoTe_2 one ($\Theta_D=135$ K). So the denominators $M_{\alpha} \langle \omega_{\alpha}^2 \rangle$ of MoTe_2 and $\text{MoTe}_{1.8}\text{S}_{0.2}$ crystals may be close. Let's pay attention to the numerator, the $N(F)$ of $\text{MoTe}_{1.8}\text{S}_{0.2}$ single crystal ($N(F)=0.88$ states/eV) is just 67 % of that of MoTe_2 one ($N(F)=1.33$ states/eV), which indicates the mean square EPC matrix element averaged over Fermi surface $\langle I_{\alpha}^2 \rangle$ of $\text{MoTe}_{1.8}\text{S}_{0.2}$ single crystal should be much larger than that of MoTe_2 one because the EPC strength λ_{ep} of $\text{MoTe}_{1.8}\text{S}_{0.2}$ ($\lambda_{ep}=0.49$) is over one and half times than that of MoTe_2 ($\lambda_{ep}=0.32$). Thus, we can propose that the improvement of superconductivity in $\text{MoTe}_{1.8}\text{S}_{0.2}$ single crystal may be related to the dramatic changing or reconstructing of the Fermi surface in the new structure induced by the substitution of Te ions by S one. However, the compressive exploration of superconductivity in $\text{MoTe}_{2-x}\text{S}_x$ from both experimental and theoretical perspectives is needed in the future.

IV Conclusion

We find that the superconductivity in MoTe_2 single crystal can be much enhanced by the

partial substitution of the Te ions by the S ones. The maximum of the superconducting temperature T_C of $\text{MoTe}_{1.8}\text{S}_{0.2}$ single crystal is about 1.3 K. Compared with the parent MoTe_2 single crystal ($T_C=0.1$ K), nearly 13-fold in T_C is improved in $\text{MoTe}_{1.8}\text{S}_{0.2}$ one. The superconductivity has been investigated by the resistivity and magnetization measurements. $\text{MoTe}_{2-x}\text{S}_x$ single crystals belong to weak coupling superconductors and the improvement of the superconductivity may be due to the enhanced EPC induced by the S-ion substitution. A dome-shape superconducting phase diagram is obtained in the S-doped MoTe_2 single crystals. The $\text{MoTe}_{2-x}\text{S}_x$ materials may provide a new platform to understand the interplay between the superconductivity and topological physics in TMDs.

Acknowledgement

This work was supported by the Joint Funds of the National Natural Science Foundation of China and the Chinese Academy of Sciences' Large-Scale Scientific Facility under contracts (U1432139, U1232139), the National Nature Science Foundation of China under contracts (51171177, 11404342), the National Key Basic Research under contract 2011CBA00111, and the Nature Science Foundation of Anhui Province under contract 1508085ME103, 1408085MA11.

Author contributions:

Y.S. proposed the work. X.L. and Y.S. designed the research. F.C. grew the single crystals. F.C. and Q.P. made the material characterizations with the help of L.L., C.X. and W.S.; R.X., D.S. and W.L. did the theoretic calculations. R.Z. carried out the Raman measurements. B. Z., H. Y. and J. L. performed the TEM measurements. F.C., X.L. and Y.S. co-wrote the paper. All authors commented to the manuscript.

References:

- [1] Dong HoonKeum, Suyeon Cho, Jung Ho Kim, Duk-Hyun Choe, Ha-Jun Sung, Min Kan, Haeyong Kang, Jea-Yeol Hwang, Sung Wng Kim, Heejun Yang, K. J. Chang, and Young Hee Lee, *Nature Physics* **11**, 482 (2015).
- [2] Suyeon Cho, Sera Kim, Jung Ho Kim, Jiong Zhao, JinbongSeok, Dong HoonKeum, JaeyoonBaik, Duk-Hyun Choe, K. J. Chang, KazuSeunaga, Sung Wng Kim, Yong Hee Lee, Heejun Yang, *Science*, **349**, 625 (2015).
- [3] Mazhar N. Ali, Jun Xiong, Steven Flynn, Jing Tao, Quinn D. Gibson, Leslie M. Schoop, Tian Liang, Neel Haldolaarachchige, Max Hirschberger, N. P. Ong, and R. J. Cava, *Nature***514**, 205 (2014).
- [4] J. T. Ye, Y. J. Zhang, R. Akashi, M. S. Bahramy, R. Arita, and Y. Iwasa, *Science***338**, 1193 (2012).
- [5] Defen Kang, Yazhou Zhou, Wei Yi, Chongli Yang, Jing Guo, Youguo Shi, Shan Zhang, Zhe Wang, Chao Zhang, Sheng Jiang, Aiguo Li, Ke Yang, Qi Wu, Guangming Zhang, Liling Sun, and Zhongxian Zhao, *Nature Commun.***6**, 6088 (2015).
- [6] Xing-Chen Pan, Xuliang Chen, Huimei Liu, Yanqing Feng, Zhongxia Wei, Yonghui Zhou, Zhenhua Chi, Li Pi, Fei Yen, Fengqi Song, Xianggang Wan, Zhaorong Yang, Baigeng Wang, Guanhou Wang, and Yuheng Zhang, *Nature Commun.***6**, 7805 (2015).
- [7] Yan Sun, Shu-Chun Wu, Mazhar N. Ali, Claudia Felser, and Binghai Yan, Preprint at <http://arXiv:1508.03501v2> (2015).
- [8] Yanpeng Qi, Pavel G. Naumov, Mazhar N. Ali, Catherine R. Rajamathi, Oleg Barkalov, Yan Sun, Chandra Shekhar, Shu-Chun Wu, Vicky Sü ß , Marcus Schmidt, EchhardPippel, Peter Werner, ReinaldHillebrand, Tobias Förster, Erik Kampertt, Walter Schnelle, Stuart Parkin, R. J. Cava, Claudia Felser, Binghai Yan, Sergiy A. Medvedev, Preprint at <http://arXiv:1508.03502> (2015).
- [9] X. Qian, J. Liu, L. Fu, and J. Li, *Science***346**, 1344 (2014).
- [10] D. E. Moncton, J. D. Axe, and F. J. DiSalvo, *Phys. Rev.* **B16**, 801 (1977).
- [11] Alexey A Soluyanov, Dominik Gresch, Zhijun Wang, Quansheng Wu, Matthias Troyer, Xi Dai, and B. Andrei Bernevig, <http://arXiv:1507.01603v1>(2015).
- [12] H. P. Hughes and R. H. Friend, *Journal of Physics C: Solid State Physics***11**, L103 (1978);

- Thorsten Zandt, HelmutDwelk, ChristophJanowitz, and RecardoManzke, *Journal of Alloys and Compounds***442**, 216 (2007).
- [13] Yan Sun, Shu-Chun Wu, Mazhar N. Ali, Claudia Felser, and Binghai Yan, *Phys. Rev. B***92**, 161107(2015).
- [14] P. Giannozzi, et al., *J. Phys.: Condens. Matter***21**, 395502 (2009).
- [15] K.F. Garrity, J.W. Bennett, K.M. Rabe, and D. Vanderbilt, *Comput. Mater. Sci.* 81, 446 (2014).
- [16] S. Grimme, *J. Comp. Chem.***27**, 1787 (2006).
- [17] V. Barone et al., *J. Comp. Chem.***30**, 934 (2009).
- [18] H. J. Monkhorst and J. D. Pack, *Phys. Rev. B* 13, 5188 (1976).
- [19] H. Padamsee, J. E. Neighbor, and C. A. Shiffman, *J. Low Temp. Phys.* 12, 387 (1973).
- [20] W. L. McMillan, *Phys. Rev.* 167, 331 (1968).
- [21] Michaela Rifliková, Roman Martoňák, and ErioTosatti, *Phys. Rev. B* 90, 035108 (2014).
- [22] L. N. Cooper, *Phys. Rev.* 104, 1189 (1956).
- [23] J. Bardeen, L. N. Cooper, and J. R. Schrieffer, *Phys. Rev.* 106, 162(1957).
- [24] J. Bardeen, L. N. Cooper, and J. R. Schrieffer, *Phys. Rev.* 108, 1175 (1957).

Table I: The physical properties of MoTe₂ and MoTe_{1.8}S_{0.2} single crystals.

Parameters	Units	MoTe ₂	MoTe _{1.8} S _{0.2}
T_C	K	0.1	1.3
γ	mJ mol ⁻¹ K ⁻²	3.06	2.07
β	mJ mol ⁻¹ K ⁻⁴	0.758	0.635
$N(E_F)$ (<i>exp.</i>)	states/eV	1.3	0.88
Θ_D	K	135	143
λ_{ep}		0.32	0.49

Figure 1:

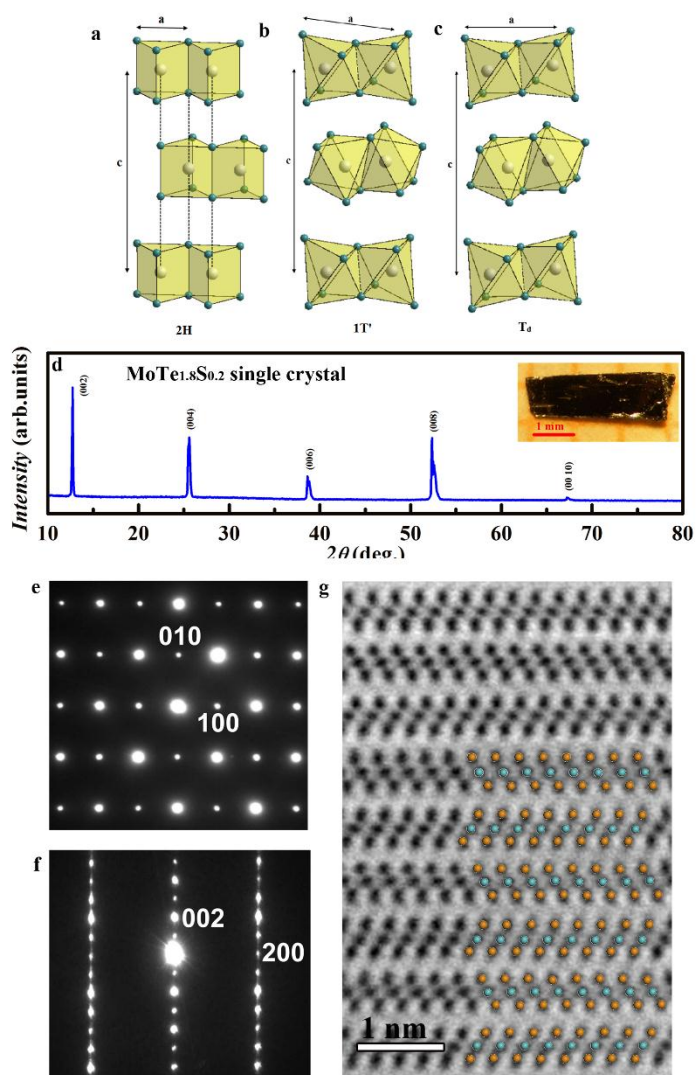


Fig. 1: (a), (b) and (c): The crystalline structure of $2H$, $1T'$ and T_d structures of MoTe_2 ; (d): XRD patterns of the $\text{MoTe}_{1.8}\text{S}_{0.2}$ single crystal measured on the (001) surface. Inset presents the picture of the single crystal used for this study. The size is approximately $3 \times 1 \times 0.5$; (e) and (f): The electron diffraction patterns of $\text{MoTe}_{1.8}\text{S}_{0.2}$ single crystal taken along [001] and [010] zone axis directions, respectively; (g) The ABF-STEM image of $\text{MoTe}_{1.8}\text{S}_{0.2}$ single crystal taken along [010] zone direction, the orange and cyan spheres represent the Te/S ions and Mo ones, respectively. Scale bar is 1nm.

Figure 2:

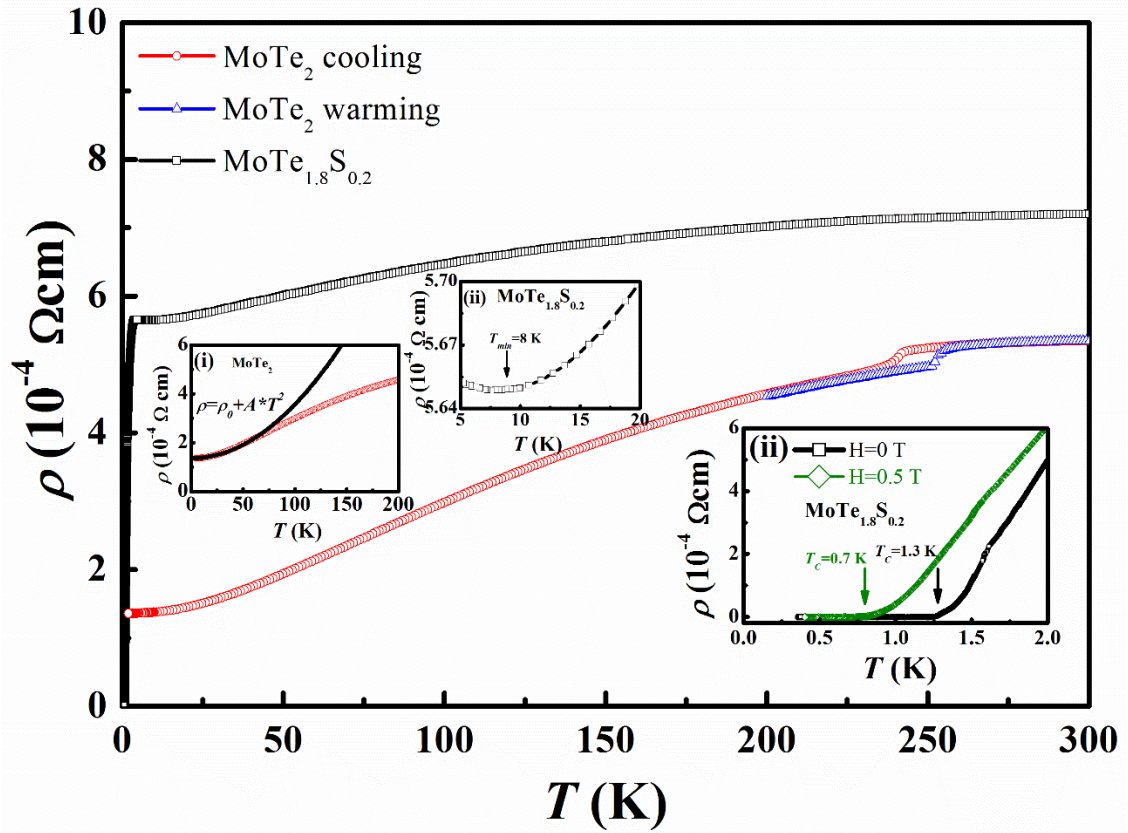


Fig. 2: The temperature dependence of resistivity of MoTe_2 (warming and cooling modes) and $\text{MoTe}_{1.8}\text{S}_{0.2}$ single crystals. The left inset presents the fitting result according to the Fermi liquid theory. The middle inset shows the minimum of the resistivity ρ_{min} with a larger scale. The right inset presents the temperature dependence of resistivity of $\text{MoTe}_{1.8}\text{S}_{0.2}$ single crystal under $H=0$ T and 0.5 T at the low temperature.

Figure 3:

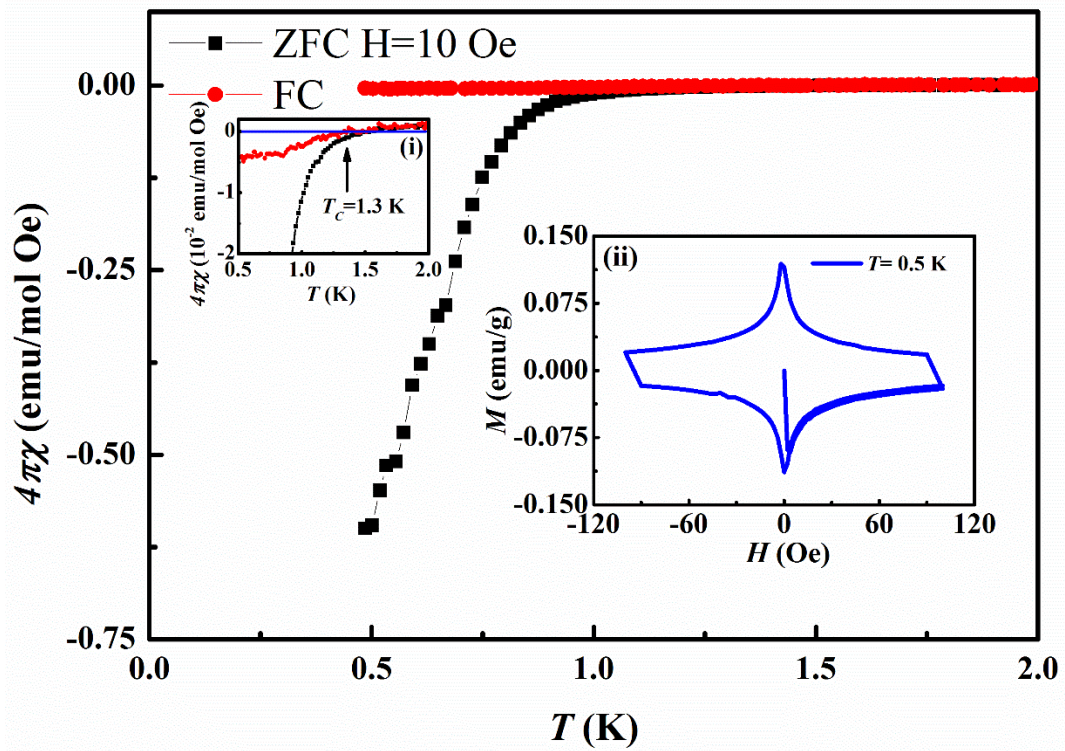


Fig. 3: The temperature dependence of magnetization of MoTe_{1.8}S_{0.2} single crystal with ZFC and FC modes under $H=10$ Oe. The left inset presents the temperature dependence of magnetization under a large scale around the T_c . The right inset shows the magnetic field dependence of magnetization at $T=0.5$ K.

Figure 4:

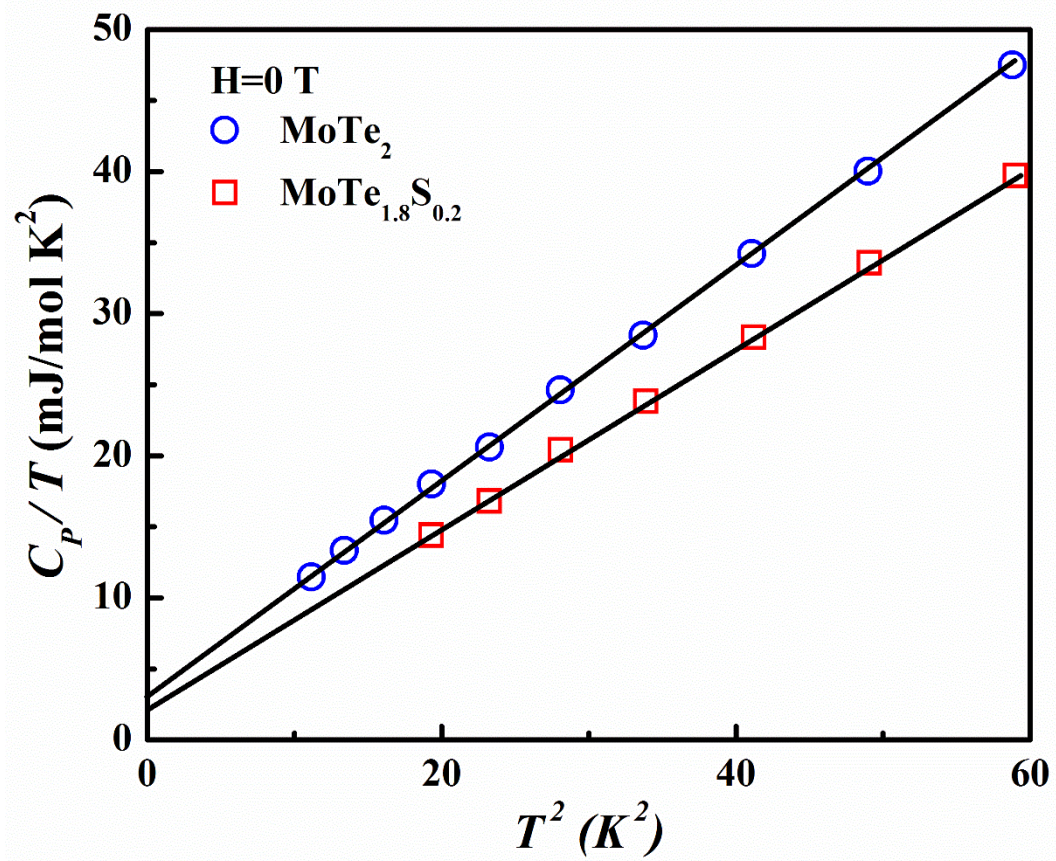


Fig. 4 : T^2 dependence of C_p/T of MoTe_2 and $\text{MoTe}_{1.8}\text{S}_{0.2}$ crystals under zero field. The solid lines show the heat capacity data fitting with the equation $C_p/T = \gamma_N + \beta T^2$.

Figure 5:

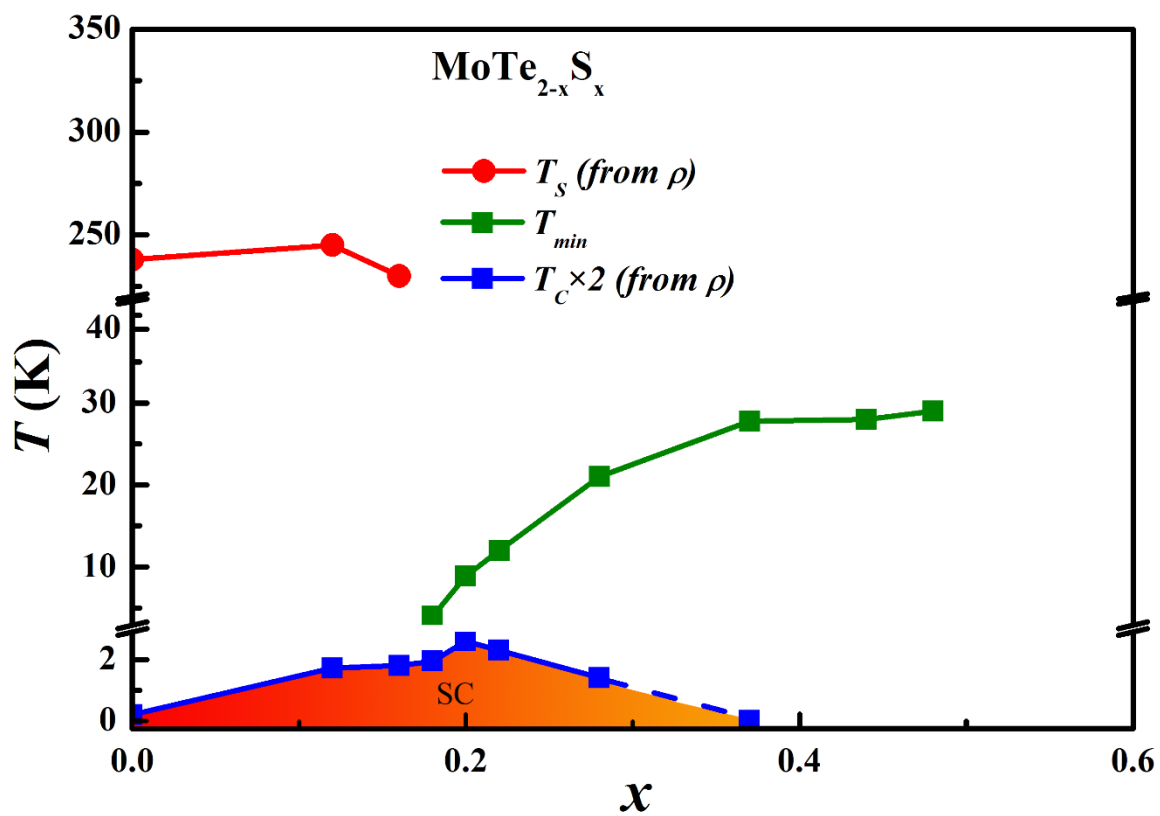


Fig. 5: The superconducting phase diagram of $\text{MoTe}_{2-x}\text{S}_x$ single crystals. SC presents the superconductivity.